Journal of Solid State Chemistry 319 (2023) 123820

Contents lists available at ScienceDirect

Journal of Solid State Chemistry

journal homepage: www.elsevier.com/locate/jssc

Tuning of band gap by anion variation of double perovskites K_2AgInX_6 (X = Cl, Br) for solar cells and thermoelectric applications

Nessrin A. Kattan [a], Syed Awais Rouf [b,*], N. Sfina [c,d], Murefah mana Al-Anazy [e], Hamid Ullah [f], A. Hakamy [g], Abeer Mera [h,i], Q. Mahmood [j,k,**], Mohammed A. Amin [l]

[a] Department of Physics, College of Science, Taibah University, Medina, Saudi Arabia
[b] Department of Physics, Division of Science and Technology, University of Education, Lahore, Pakistan
[c] College of Sciences and Arts in Mahayel Asir, Department of Physics, King Khalid University, Abha, Saudi Arabia
[d] Laboratoire de la Matière Condensée et des Nanosciences (LMCN), Université de Monastir, Département de Physique, Faculté des Sciences de Monastir, Avenue de l'Environnement, 5019, Monastir, Tunisia
[e] Department of Chemistry, College of Sciences, Princess Nourah bint Abdulrahman University (PNU), P.O. Box 84428, Riyadh, 11671, Saudi Arabia
[f] Dartment of Physics, Riphah International University, Campus Lahore, Pakistan
[g] Department of Physics, Faculty of Applied Science, Umm Al-Qura University, Makkah, 21955, Saudi Arabia
[h] Department of Physics, College of Arts and Science, Prince Sattam Bin Abdulaziz University, Wadi Addawasir, 11991, Saudi Arabia
[i] Department of Physics, Faculty of Science, Kafrelsheikh University, Kafrelsheikh, 33516, Egypt
[j] Basic and Applied Scientific Research Center, Imam Abdulrahman Bin Faisal University, P.O. Box 1982, Dammam, 31441, Saudi Arabia
[k] Department of Physics, College of Science, Imam Abdulrahman Bin Faisal University, P.O. Box 1982, Dammam, 31441 Saudi Arabia
[l] Department of Chemistry, College of Science, Taif University, P.O. Box 11099, Taif, 21944, Saudi Arabia

ARTICLE INFO

Keywords:
Solar cells
Visible region
Thermoelectric properties
Figure of merit
Lattice thermal conductivity

ABSTRACT

In recent research double perovskites have become the burning topic for solar cells because of lead free nature, stability, and exceptional performance. Therefore, here we have explained the optical and transport properties of K_2AgInX_6 (X = Cl, Br) for solar cells and thermoelectric generators. The confirmation of thermodynamic stability been reported by formation energy and structural existence by tolerance factor. The band gaps of 2.34 eV, 1.37 eV, and 0.0 eV are computed from the band structures for $K_2AgInCl_6$, $K_2AgInBr_6$, and K_2AgInI_6, respectively. The band gap of $K_2AgInBr_6$ is found ideal for solar cells having large absorption band (376–612 nm) in the visible region. The optical characteristics of $K_2AgInCl_6$, and $K_2AgInBr_6$ are argued in terms of dielectric constants, refractive index, optical loss, and reflection of light. Finally, the thermoelectric behavior has been described by power factor and figure of merit in terms of carrier's concentration and temperature. The large Seebeck coefficient and remarkably small lattice conductivity increases their significance for thermoelectric generators.

1. Introduction

From the last few decades, the researchers have been struggling to find sustainable clean and green energy alternatives to rapidly dying conventional sources of energy. Because energy production cost and usage has been increasing day by day along with causing adverse environmental pollution [1–3]. Sunlight and heat being easily available in the most part of the world through-out the year are the cheaper alternatives to the energy resources like fossil fuels [4]. At present, one of the important green energy sources is the solar cell. It has been considered an efficient alternative to fossil fuels having low production costs and high performance [5]. Solar cell technology depends mainly on the material used for the manufacturing of solar cells, because different materials have shown different energy conversion efficiencies [6]. Therefore, advanced systematic attempts are required to find efficient, cost-effective and stable, as well as sustainable solar cells. Perovskite solar cells (PSCs) have been developed and extensively tested by many researchers [6–11] to study environmental effects (like moisture and heat, etc.) on the performance of PSC [9–11]. Poor stability and toxic nature of Pb-based perovskites have been the major hindrance in the large-scale production, as reported by many researchers [12]. Perovskites have shown absorption of visible light energy, which undoubtedly proposes their

* Corresponding author.
** Corresponding author. Basic and Applied Scientific Research Center, Imam Abdulrahman Bin Faisal University, P.O. Box 1982, Dammam, 31441, Saudi Arabia.
E-mail addresses: syedawais.rouf@ue.edu.pk (S.A. Rouf), qmmustafa@iau.edu.sa (Q. Mahmood).

https://doi.org/10.1016/j.jssc.2022.123820
Received 6 September 2022; Received in revised form 15 December 2022; Accepted 21 December 2022
Available online 27 December 2022

future usage in solar cell technology [13].

Double perovskites have appeared as an important alternative to many other solar cell materials due to efforts of researchers for growth of Pb-free perovskite solar cells for their usage in photovoltaics on commercial scale. Double-perovskites having formula AB'B″X_6 (A, B′, and B″ are metal cations and X is an anion) have helped researchers in development of research fields of photovoltaics, photocatalysis, optoelectronics and thermoelectrics [14]. Liu et al., in 2015 [15] reported that lead-based organic perovskites have shown high efficiency 22.1% but due to toxicity of Pb and instability of structure, their applications are limited. Nevertheless, many other Pb-free perovskites, for example, Murtaza et al. [16,17], has investigated double perovskites, i.e., $Rb_2AgTlCl_6$ and $Cs_2AgTlCl_6$, and reported to have high stability along with high absorption. In Refs. [18,19], Rb_2TeA_6 (A = Cl, Br, I) have been studied using first-principle approach. Also, Mahmood et al. [20] has reported promising optoelectronic and thermoelectric properties of cubic Rb_2PtY_6 (Y = Cl, Br) double perovskite. There have been efforts made by various researchers [21–23] to develop organic-inorganic hybrid perovskites of the form $CH_3NH_3PbX_3$ (X = Cl, Br, I) due to their less weight and easy fabrication. These hybrid perovskites have shown critical toxicity and stability issue and are in use currently for limited solar systems [24,25]. Consequently, researchers have been focusing on the development of Pb-free double perovskites. Recently, many researchers [26–28] have reported many lead-free non-toxic and stable materials for renewable energy applications, i.e., solar cells, photovoltaics, and light emitting diodes (LED's), as well as thermoelectric (TE) generators.

In Ref. [29], $Cs_2InAgCl_6$ was studied and reported direct bandgap of 3.3 eV and ZT value of 0.94 suitable for thermoelectric devices. Tariq et al. [30] has studied Cs_2AgInY_6 (Y = Cl, Br, I, F) and emphasized on semiconducting nature and direct bandgap of these materials. Khan et al. [31] has investigated the opto-electronic and transport properties of Cs_2ScAgY_6 (Y = Cl, Br, I). These compounds have shown indirect bandgap value of 1.9 eV and 1.55 eV, along with figure of merit value of 0.74 at 300 K. Nawaz et al. [32] has reported DFT studies of Rb_2YInA_6 (A = I, Br, Cl) and highlighted their potential usage in optoelectronic and cooling thermal devices. Nazir et al. [33] has studied $X_2LiInBr_6$ (X = Rb, Cs) for solar cell applications. Anbarasan et al. [34] reported structural, mechanical, and optoelectronic characteristics of Cs_2AgInY_6 (Y = Cl, Br, I) using first-principle calculations. Mukhtar et al. [35] studied X_2NaInI_6 (X = Cs, Rb) double perovskite and found them to be suitable for solar cell fabrication. Noor et al. [36] has analyzed X_2ScInI_6 (X = Rb, Cs) using DFT and found them useful for optoelectronic devices. Iqbal et al. [37] studied opto-electronic and thermoelectric properties of Rb_2AlInX_6 (X = Cl, Br, I) using DFT. The studied DPs K_2AgInX_6 (X = Cl, Br) are highly stable, and have direct band gap which is important for inter-band transitions and recombination's. The $K_2AgInBr_6$ has ideal band gap (1.30 eV) for solar cells with large absorption energy band in the visible region. Therefore, $K_2AgInBr_6$ is very much important for high performance inorganic materials to fabricate solar cells. Furthermore, the large values of Seebeck coefficient and ultralow thermal conductivity increases the figure of merit at low and room temperature. Therefore, our findings will provide deep knowledge and excellent materials to experimental researchers to realize them for renewable energy.

In light of above literature, we have addressed the structural, electronic, optical, and thermoelectric characteristics of DPs K_2AgInX_6 (X = Cl, Br, I) for solar cells and energy harvesting applications which increase their importance. The tunning of band gaps by varying anions Cl to I shifts the absoption regions from ultraviolet to visible region. Therefore, our findings provides evidences to researchers to realize them for solar cells applications.

2. Method of calculations

Computations have been performed for K_2AgInX_6 (X = Cl, Br) DPs by using Wien2K code with employing FP-LAPW method [38,39]. The PBE-GGA functional was used for calculating precise lattice constants, ground state energy and bulk modulus though Murnaghan's equations of states for studied DPs [40–42]. This approximation helps in computing the structural parameters; however, it underestimates the electronic parameters specially band gap. The TB-mBJ potential is versatile and take less time for calculation as compared to Hybrid functional HSE06, even though, these two potentials have equivalent accuracy [43]. Therefore, to accurate the band gap, the TB-mBJ potential is applied over PBE-GGA. Furthermore, the SOC coupling has also been included because it affects the band gap materials of heavy elements. For calculations, the following input values of $\ell_{max} = 10$, $G_{max} = 14$ and $R_{MT} \times K_{max} = 8$ are inserted in the software. To obtain converged parameters, the k-mesh of $15 \times 15 \times 15$ was used and convergence is set at 10^{-5} Ry. The BoltzTrap code is used for calculation of thermoelectric properties and lattice thermal conductivity by ShengBTE code [44].

3. Results and discussion

3.1. Structural properties

The crystal structures of cubic phase DPs K_2AgInX_6 (X = Cl, Br, I) with space group Fm $\overline{3}$ m (225) are plotted in Fig. 1 whose lift side has atomic view and right-side polyhedral form. The region among the octahedra AgX_6 and InX_6 is occupied by the base element K which is represented by blue balls. The octahedra separate each other by 6-fold of coordination of X atoms. Therefore, the 12 and 6 atoms of anions (Cl, Br, I) covers the central atoms (Ag, In) and K atoms, respectively. The each octahedra has Ag (dark blue) and In (purple) atoms at the center surrounded by halide ions (Cl, Br, I) in green color. In this way the 4a, 4b, 8c and 24e Wyckoff sites are associated with Ag, In, K and X atoms, respectively [45]. These Wyckoff sites have the coordination positions (0, 0, 0), (0.25, 0.25, 0.25), and (0.2, 0, 0) which illustrate the atomic existence.

The crystal structures in cubic phase are optimized to get the lattice constant (a_0), energy released (E), and bulk modulus (B) though Murnaghan's equation of states. The calculated values are given in Table 1, which instigate the a_0 increases from Cl to I due to increasing size of halogen atoms. Furthermore, B decreases from Cl to I due to increasing a_0 reduces the ability of the materials to bear stress. For the calculations of formation energy, the individual elements, and compounds structures are optimized, and their energies are fitted in the chemical relation

$$\Delta H_f = E_{Total}(K_l Ag_m In_n X_o) - lE_K - mE_{Ag} - nE_{In} - oE_X \quad (1)$$

Here $E_{Total}(K_l Ag_m In_n X_o)$ is the total energy of K_2AgInX_6 while E_K, E_{Ag}, E_{In} and E_X are the energies of K, Ag, In and X atoms [46]. The negative values of ΔH_f for the studied DPs confirm their thermodynamic stability (See Table 1). It decreases from Cl to I which shows the decrease in thermodynamic stability. Furthermore, the structural stability has also been calculated from

$$t_F = \frac{r_K + r_X}{r_B + r_X} \quad (2)$$

Here r_K, r_B and r_X are the radii of K, B = Ag + In/2, and X atoms. The value of B is calculated by taking the average of Ag and In atoms atomic radii. The radii of the elements are calculated from the Xcrysden software by taking the optimized structures. The stable compounds have the range of t_F from 0.90 to 1.0 [47]. The computed values are 0.94 and 0.95 for $K_2AgInCl_6$ and $K_2AgInBr_6$, respectively. Therefore, the studied DPs structures are stable (See Table 1) and can be used for characterization to explore their applications.

3.2. Electronic properties

The electronic characteristics of these studied DPs are analyzed from BS as highlighted in Fig. 2 (a-c). It is clear that the valence band (VB) uper edge and conduction band (CB) lower edge lie at Γ direction that show

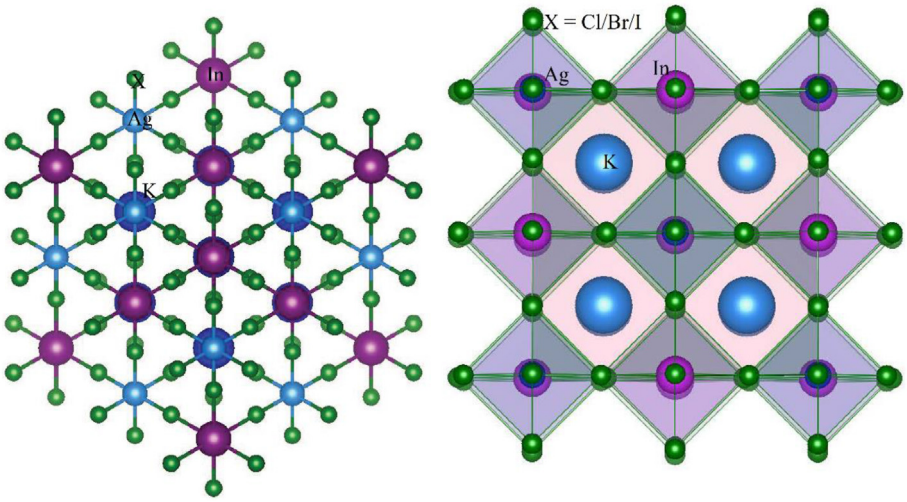

Fig. 1. Crystal structure of K_2AgInX_6 (X = Cl, Br, I) in atomic (left side) and polyhedral form (right side).

Table 1
The lattice and optical parameters of K_2AgInX_6 (X = Cl, Br, I).

Parameter	$K_2AgInCl_6$	$K_2AgInBr_6$	K_2AgInI_6
a_o (Å)	10.32	10.86	11.79
B_o (GPa)	36.90	27.63	23.14
H_f (eV)	−1.66	−1.08	−0.86
T_f	0.94	0.95	0.97
E_g (eV)	2.37	1.34	0.0
$\varepsilon_1(0)$	2.61	3.20	6.22
n(0)	1.61	1.79	2.49
R (0)	0.055	0.079	0.183
m_e^*	$0.23m_0$	$0.25m_0$	$0.34m_0$
m_h^*	$0.18m_0$	$0.20\ m_0$	$0.27\ m_0$

the direct band gap. The direct band gap is essential for optoelectronics and solar cells. The values of band gaps for $K_2AgInCl_6$, $K_2AgInBr_6$, and K_2AgInI_6 are 2.37 eV, 1.34 eV, and 0.0 eV, respectively. The band gap 2.37 eV for $K_2AgInCl_6$ ensure the absoprtion from visible to ultravioet region, 1.34 eV for $K_2AgInBr_6$ has ideal range which lies in visible region and zero band gap for K_2AgInI_6 shows the metallic behavior. Moreover, the states are flat and dense at VB and states at CB are curved and very less which show the holes are effective masess are larger and moble carriers are electrons in the studied DPs. The calculated effective masses of electrons (m_e^*) and holes (m_h^*) at conduction and valence band edges are shown in Table 1 which show the holes have large values of m_h^* as compared to electrons m_e^*. Therefore, our calculated results are consistent with discription of band structures.

For the comprehensive analysis of contribution of carriers, transitions and recombination, the DOS of individual elements are essential. Therefore, the DOS of K, Ag, In and X atoms are drawn in Fig. 3 (a-c). The s, p states of K lies in energy range of −1.5 to −3.0 eV, −1.0 to −2.0 eV, and E_F to −1.5 eV for $K_2AgInCl_6$, $K_2AgInBr_6$, K_2AgInI_6, respectively in the VB. In the CB, the states exist from 7.0 to 8.0 eV for $K_2AgIn(Cl/Br)_6$, and 4.0–8.0 eV for K_2AgInI_6. These are deep level states and their impact on the physical characteristics of materials is negligible. Furthermore, the s, p, d states of Ag falls in the range −3.0 to −3.5 eV, −2.0 to −3.0 eV, and zero to −3.5 eV in VB while in CB, the states exists 5.5–7.0 eV, 2.5–4.0 eV, and at E_F for $K_2AgInCl_6$, $K_2AgInBr_6$, and K_2AgInI_6, respectively. Furthermore, the p, d states of In lie from E_F to −3.5 eV in VB and in CB their contribution is ignorable. Finally, the X (Cl, Br, I) atoms' p states exists from E_F to −3 eV in the VB and some portion from 2.0 to 3.0 eV in CB. However, its s states across the E_F level for K_2AgInI_6. Therefore, the analysis reveals that the favorable transitions occur from d states of Ag, p, d states of In and p states of X atoms to d states of Ag and p states of X atoms for $K_2AgInCl_6$ and $K_2AgInBr_6$. For K_2AgInI_6 the states show the intra-band transitions and metallic character. Therefore, we have only elaborated the optical and thermoelectric properties of $K_2AgInCl_6$ and $K_2AgInBr_6$.

3.3. Optical properties

The optical characteristics of K_2AgInX_6 (X = Cl, Br) are discussed by dielectric constants $\varepsilon(\omega) = \varepsilon_1(\omega) + i\varepsilon_2(\omega)$ and their dependent parameters. Here $\varepsilon_1(\omega)$ and $\varepsilon_2(\omega)$ are real and imaginary portions which investigate the polarization/dispersion, and absorption of light energy. The

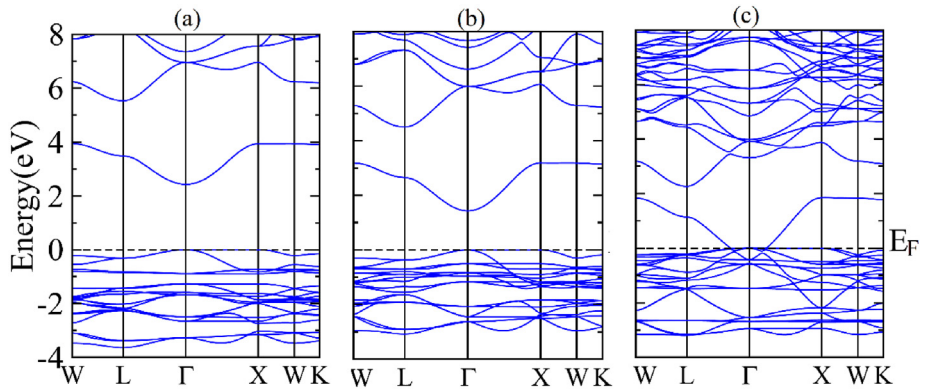

Fig. 2. The band structures of (a) $K_2AgInCl_6$, (b) $K_2AgInBr_6$, (c) K_2AgInI_6.

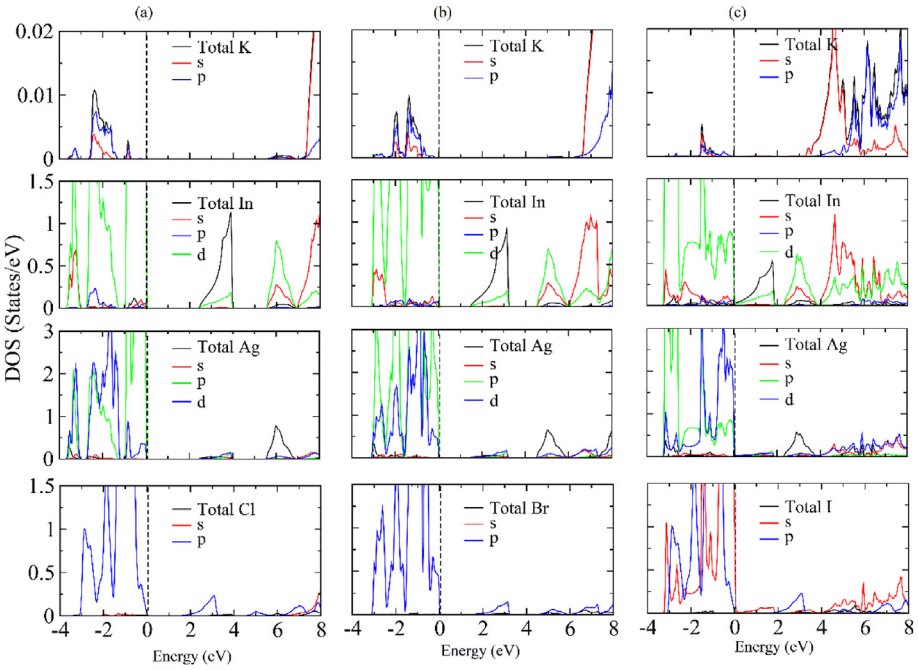

Fig. 3. Density of states of K, Ag, In and Cl/Br/I for (a) $K_2AgInCl_6$, (b) $K_2AgInBr_6$, (c) K_2AgInI_6.

refractive index n (ω), absorption α (ω) and reflection R (ω) are computed through the relation as calculated in refs [48–50]. The computed optical parameters are enclosed in Fig. 4(a–d) and Fig. 5 (a, b). The static ε_1 (0) have values 2.61 and 3.20 for $K_2AgInCl_6$ and $K_2AgInBr_6$, respectively. These static values are related to band gaps according to Penn's relation $\varepsilon_1(0) \approx 1 + (\hbar\omega_p/E_g)^2$ [51]. Its value increases and reaches to peak at 3.6 eV and 2.5 eV for $K_2AgInCl_6$ and $K_2AgInBr_6$, respectively. At resonance, the dispersion of incoming light energy is maximum and then drops to lowest values as energy slightly increase from resonance values. Furthermore, the variation in dispersion of light occurs with increase in energy. The insertion of Br-ion shows more dispersion as compare to Cl-ion. Hence, variation of anion has great importance to enhance optical applications.

Another important aspect for optical applications is refractive index n(ω), which tells about transparency of the materials. The findings of

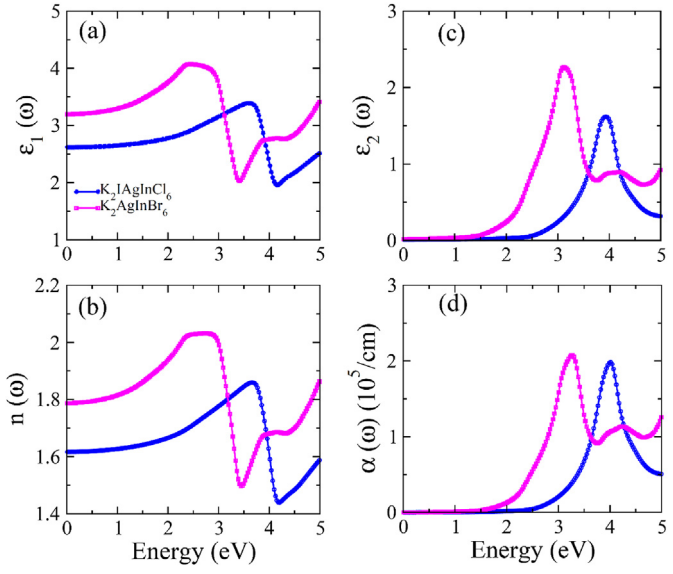

Fig. 4. The calculated (a) ε_1 (ω), (b) n (ω), (c) ε_1 (ω) and (d) α (ω) for K_2AgInX_6 (X = Cl, Br).

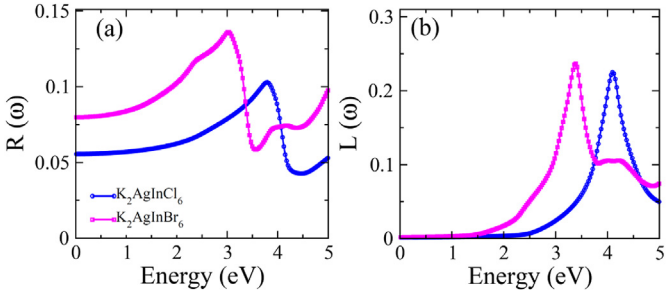

Fig. 5. The calculated (a) R (ω), and (b) L (ω) for K_2AgInX_6 (X = Cl, Br).

n(ω) reveal that its static values have relation with static dielectric constant $n_0^2 = \varepsilon_1(0)$ [52] as shown in Table 1. The increase in incident energy increases dispersion up to 3.5 and 2.5 for $K_2AgInCl_6$ and $K_2AgInBr_6$, respectively, as presented in Fig. 4b.

The ε_2(ω) measures the absorption of light energy whose obtained values are drawn in Fig. 4 (c). The ε_2(ω) is computed from ε_1(ω) through Kramer–Kronig relation [53]. Its threshold values show the optical band gap which is determined by drawing tangent to the curves. These optical band gaps 2.37 eV and 1.35 eV are consistent with band gaps computed from BS which ensure the reliability of the theoretical calculations of BS and optical analysis. It is noticed that the maximum absorption bands fall in the energy range from 3.0 eV to 4.5 eV and 2.0 eV–3.5 eV for $K_2AgInCl_6$, and $K_2AgInBr_6$, respectively. Therefore, the $K_2AgInCl_6$ is suitable for optoelectronic devices in ultraviolet regions whereas $K_2AgInBr_6$ is significantly important for solar cells in working in visible region. Similarly, α (ω) also show the absorption of light energy as depicted in Fig. 4 (d). It is clear from the graphs the absorption bands are consistent with the absorption bands found in ε_2(ω).

Like above discussion of optical parameters reflectivity R(ω) and optical loss L(ω) are also important factors whose values should be minimum for best optical materials. The R(ω) illustrate the surface morphology of studied compounds. Computed values of R(ω) are shown in Fig. 5a. Its values at zero energy are 0.055 and 0.079 for $K_2AgInCl_6$, and $K_2AgInBr_6$, respectively. It increases with rising the energy of photons and becomes maximum at 3 eV (0.10) and 3.6 eV (0.14). The L(ω) is

demonstrate the dispersion and scattering of light as presented in Fig. 5b. $K_2AgInBr_6$ and $K_2AgInCl_6$ are good materials in the energy range 1 eV–1.7 eV and 1 eV–2.2 eV, respectively. The increase in energy, loss also increases and gain maximum loss at 3.2 eV and 4.2 eV for $K_2AgInBr_6$ and $K_2AgInCl_6$, respectively. The above discussion ensure that the $K_2AgInBr_6$ is more important for solar cells than $K_2AgInCl_6$ because of least energy loss and large values of absorption in the visible region.

3.4. Thermoelectric properties

We have characterized our studied compounds for their thermoelectric performance from figure of merit (ZT) as given by $ZT = (\sigma S^2/k)$ [54–56]. An efficient thermoelectric material has high Seebeck coefficient (S), high electrical conductivity (σ), and low thermal conductivity (κ). We have utilized BoltzTrap code to compute thermoelectric properties of $K_2AgInCl_6$ and $K_2AgInBr_6$ with respect to temperature T (K) and chemical potential μ (eV). The p- and n-type characters have been categorized by carrier's concentration. The μ tells us about the energy needed for the addition or removal of electrons from the materials. The μ is positive when electrons are added to the system and it is negative when electrons are removed from the system. When electrons are added in the system, it acts as n-type material and removal of electrons increase holes which shows the studied materials are p-type [57]. Furthermore, the DOS are largely occupied at the valence band than at the conduction band (Fig. 3) that confirm the presence of holes as dominant charge carriers and p-type nature. The density of states represents the probability of existence of carriers. The valence band has large number of closely spaced density of states as compared to conduction band which shows the more carriers are available at valence band than conduction band. In semiconductors if the holes are majority carriers VB than electrons in the CB the behaviors become the p-type. The computed values of σ and κ_e against μ and T are drawn in Fig. 6(a-d). The calculated σ values are shown in Fig. 6a that includes the carrier's concentration for μ ranges from −0.15 eV to 0.30 eV. The first peaks of σ for $K_2AgIn(Cl/Br)_6$ are found at −0.03/0/-0.04 eV with intensity of carriers 5.0/6.0 × 10^5 ($\Omega^{-1}m^{-1}$) in p-type and at 0.24/0.18 eV with intensity of carriers 7.5/7.8 × 10^5 ($\Omega^{-1}m^{-1}$) in n-type region. In the core side from −0.1 eV to −0.15 eV the intensity of carriers reaches to 5.0/6.0 × 10^5 ($\Omega^{-1}m^{-1}$) but these carriers are not actively contributed to the σ. The computed σ values at 100 K is about 0.30/0.26 × 10^5 ($\Omega^{-1}m^{-1}$) and reaches to 1.0/1.1 × 10^5 ($\Omega^{-1}m^{-1}$) at 500 K for $K_2AgIn(Cl/Br)_6$ (c.f., Fig. 6b), because high kinetic energy electrons break bonds at high temperature. The σ of $K_2AgInCl_6$ is relatively more than $K_2AgInBr_6$ at each point due to electrons of $K_2AgInCl_6$ facing less collision.

The thermal conductivity (κ) has two parts, i.e., electronic (k_{el}) and phonon (k_{ph}) part. The impact of phonons has been ignored because of high computational cost and restrictions of BoltzTraP code. The obtained κ_e values are plotted for μ and T in Fig. 6(c and d) that show analogous results to σ but having extremely low intensities. The κ_e rises from 0.15/0.14 (W/mK) at 100 K up to 2.40/2.45 (W/mK) at 500 k for both $K_2AgIn(Cl/Br)_6$. However, the κ_e is 10^5 smaller than σ that highlights potential of studied materials for solar cells applications [58].

The S is measured from ratio of potential difference (ΔV) to temperature gradient (ΔT) amid the contacts of two metals. The computed S are drawn in Fig. 7 (a, b). Its values vary from 0.04 eV to 0.15 eV for $K_2AgInCl_6$, and 0.03 eV–0.10 eV for $K_2AgInBr_6$. These values show that S has larger in n-type region due to less σ. The S for $K_2AgIn(Cl/Br)_6$ first increases slightly up to 200 K and then decreases gradually to 500 K, respectively. The values of S are larger for $K_2AgInBr_6$ than $K_2AgInCl_6$ because of small σ values as already addressed in Fig. 6 (a, b). Furthermore, the $S^2\sigma$ has been plotted to guess the thermoelectric strength of studied DPs whose values reaches to peak at 0.02 eV and in the periphery of −0.010 eV in p-type side while in n-type side the values exist at 0.27 eV and 0.21 eV for $K_2AgIn(Cl/Br)_6$. Furthermore, the PF is 1.0 W/mK^2 at 100 K and increases to 3.5 W/mK^2 which show at higher T the strength is higher due to large σ.

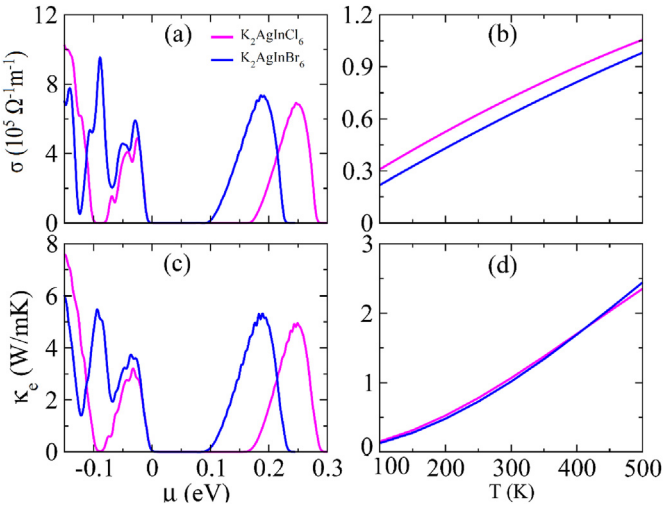

Fig. 6. The (a, b) σ, and (c, d) κ_e versus μ and T for K_2AgInX_6 (X = Cl, Br).

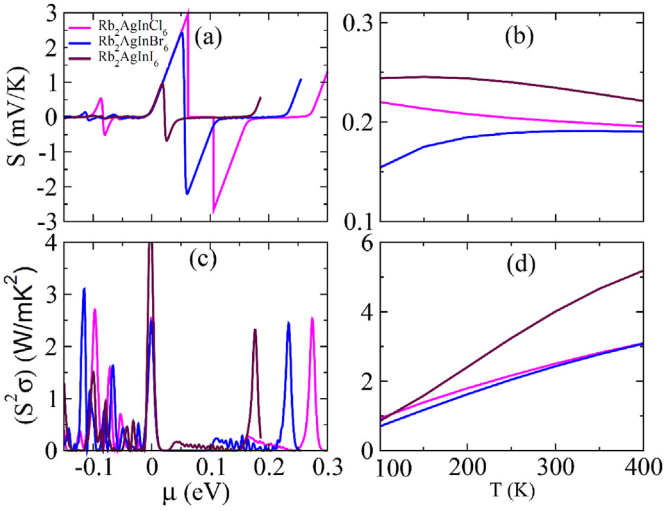

Fig. 7. The (a, b) S, and (c, d) σS^2 versus μ and T for K_2AgInX_6 (X = Cl, Br).

ZT values against μ and T has been presented in Fig. 8 (a, b). The $K_2AgInCl_6$ values are unity at 0.15 eV and 0.30 eV, whereas $K_2AgInBr_6$ value is unity at 0.07 eV and 0.2 eV, and at Fermi level. Hence for the n-type region is important because of large value of S. For both $K_2AgIn(Cl/Br)_6$, value of S decreases from 2.1/2.0 to 0.49 with increasing temperature from 100 K to 500 K. Therefore, the studied DPs have large of ZT at room temperature. The above discussion reveals the studied DPs are important for thermoelectric generators and other thermoelectric applications.

Furthermore, the specific heat capacity C_v is computed to guarantee the stability of studied DPs as shown in Fig. 8 (c, d). The contribution to C_v in the p-type region from zero to −0.15 eV is reaches to 24/29 J/mol.K while in the n-type region contribution is negligible. Therefore, holes absorb more heat as compared to electrons because of their heavy weight. Its trends against T increases from 100 K to 500 K which shows with increasing T heat capacity also increases.

The contribution of lattice thermal conductivity (κ_ℓ) is a very important parameter to determine the performance of thermoelectric materials. The computed κ_ℓ has been plotted in Fig. 9 versus T. For best thermoelectric materials, its value should be least to enhance the ZT. Its values are 2.9 W/mK and 2.5 W/mK at 100 K for $K_2AgInCl_6$, and $K_2AgInBr_6$, respectively which decreases to almost zero values at 400 K. These ultralow values are comparable with thermoelectric players as

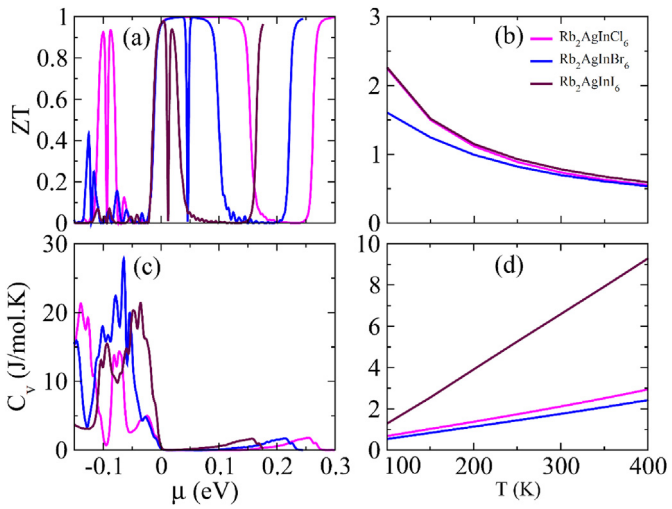

Fig. 8. The (a, b) ZT, and (c, d) C_v versus μ and T for K_2AgInX_6 (X = Cl, Br).

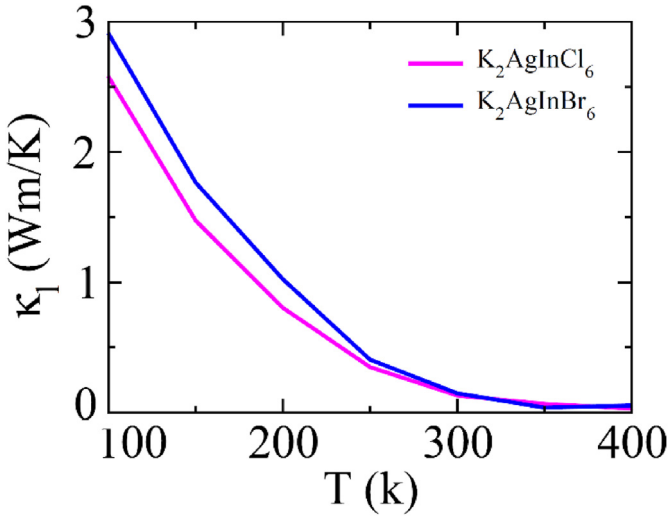

Fig. 9. Lattice thermal conductivity versus T of K_2AgInX_6 (X = Cl, Br).

0.15 W/mK [59], 1.24 W/mK [60], and 2.60 W/mK [61]. for Cs_2PdI_6, Bi_2Te_3 and GeTe, respectively.

4. Conclusion

In brief, the K_2AgInX_6 (X = Cl, Br, I) are elaborated for structural and electronic properties by DFT approach which show the $K_2AgInCl_6$ and $K_2AgInBr_6$ are direct band gap semiconductors while K_2AgInI_6 is metal. The values of t_F show the structural existence and values of ΔH_f show thermodynamic stability. The band gaps of 2.37 eV and 1.34 eV for $K_2AgInCl_6$ and $K_2AgInBr_6$ ensures their applications for ultraviolet and visible light applications. The absorption band from 376 to 612 nm for $K_2AgInBr_6$ makes it an excellent candidate for solar cells. The least values of optical loss and reflection with large attenuation of light in the visible region which favor the solar cells. The large values of ZT and PF in at low temperature and 300 K along with ultralow value of lattice vibration are outstanding parameters for thermoelectric generators applications. Therefore, the above conclusions of studied DPs will offer deep insight to the experimental community to realize them for boosting the solar cells and thermoelectric generators industry.

CRediT authorship contribution statement

Syed Awais Rouf: Conceptualization, Writing – original draft, Writing – review & editing. **N. Sfina:** Data curation, Investigation, Methodology. **Murefah mana Al-Anazy:** Data curation, Investigation, Methodology. **Hamid Ullah:** Funding acquisition, Resources, Writing – original draft. **A. Hakamy:** Funding acquisition, Resources, Writing – original draft. **Abeer Mera:** Funding acquisition, Resources, Writing – original draft. **Q. Mahmood:** Writing – original draft, Writing – review & editing, Supervision, Writing – review & editing. **Mohammed A. Amin:** Writing – original draft, Writing – review & editing, Supervision, Writing – review & editing.

Declaration of competing interest

The authors declare that they have no known competing financial interests or personal relationships that could have appeared to influence the work reported in this paper.

Data availability

Data will be made available on request.

Acknowledgement

This research was funded by the Princess Nourah bint Abdulrahman University Researchers Supporting Project number (PNURSP2022R7), Princess Nourah bint Abdulrahman University, Riyadh, Saudi Arabia. The authors extend their appreciation to the Deanship of Scientific Research at King Khalid University for funding this work through research groups program under grant number (RGP.2/145/43). The authors would like to thank Taif University Researchers Supporting Project number (TURSP-2020/03), Taif University, Taif, Saudi Arabia for supporting this project.

References

[1] S. Haid, W. Benstaali, A. Abbad, B. Bouadjemi, S. Bentata, Z. Aziz, Thermoelectric, structural, optoelectronic, and magnetic properties of double perovskite Sr_2CrTaO_6: first principle study, Mater. Sci. Eng. B 245 (2019) 68–74.
[2] M. Hussain, M. Rashid, A. Ali, M.F. Bhopal, A.S. Bhatti, Systematic study of optoelectronic and transport properties of cesium lead halide (Cs_2PbX_6; X = Cl, Br, I) double perovskites for solar cell applications, Ceram. Int. 46 (13) (2020) 21378–21387.
[3] I.S. Roqan, K.P. O'Donnell, R.W. Martin, P.R. Edwards, S.F. Song, A. Vantomme, Identification of the prime optical center in GaN: Eu^{3+}, Phys. Rev. B 81 (8) (2010), 085209.
[4] K.C. Bhamu, A. Soni, J. Sahariya, Revealing optoelectronic and transport properties of potential perovskites Cs2PdX6 (X= Cl, Br): a probe from density functional theory (DFT), Sol. Energy 162 (2018) 336–343.
[5] S.A. Khandy, D.C. Gupta, Electronic structure, magnetism and thermoelectric properties of double perovskite Sr2HoNbO6, J. Magn. Magn Mater. 458 (2018) 176–182.
[6] K. Lorenz, S.M.C. Miranda, E. Alves, I.S. Roqan, K. P O'Donnell, M. Boćkowski, High pressure annealing of Europium implanted GaN, Gallium Nitride Materials and Devices VII 8262 (2012), 82620C.
[7] G. Volonakis, A.A. Haghighirad, R.L. Milot, W.H. Sio, M.R. Filip, B. Wenger, et al., Cs2InAgCl6: a new lead-free halide double perovskite with direct bandgap, J. Phys. Chem. Lett. 8 (2017) 772–778.
[8] B.K. Ghosh, T.K. Biswas, Emerging solar cells energy trade-off: interface engineering materials impact on stability and efficiency progress, Int. J. Energy Res. 43 (2019) 1670–1688.
[9] N. Mariotti, M. Bonomo, L. Fagiolari, N. Barbero, C. Gerbaldi, F. Bella, C. Barolo, Recent advances in eco-friendly and cost-effective materials towards sustainable dye-sensitized solar cells, Green Chem. 22 (2020) 7168–7218.
[10] M.C. Jung, S.R. Raga, Y. Qi, Properties and solar cell applications of Pb-free perovskite films formed by vapor deposition, RSC Adv. 6 (2016) 2819.
[11] S. Galliano, F. Bella, M. Bonomo, G. Viscardi, C. Gerbaldi, G. Boschloo, C. Barolo, Hydrogel electrolytes based on xanthan gum: green route towards stable dye-sensitized solar cells, Nanomaterials 10 (2020) 1585.
[12] E. Pulli, E. Rozzi, F. Bella, Transparent photovoltaic technologies: current trends towards upscaling, Energy Convers. Manag. 219 (2020), 112982.

[13] F. Bella, L. Porcarelli, D. Mantione, C. Gerbaldi, C. Barolo, M. Grätzel, D. Mecerreyes, A water-based and metal-free dye solar cell exceeding 7% efficiency using a cationic poly(3,4-ethylenedioxythiophene) derivative, Chem. Sci. 11 (2020) 1485–1493.

[14] M.A. Bavio, J.E. Tasca, G.G. Acosta, M.F. Ponce, R.O. Fuentes, A. Visintin, Study of double perovskite La2B(II)MnO6 (B: Ni, Co, Cu) as electrode materials for energy storage, J. Solid State Electrochem. 24 (2020) 699–710.

[15] X. Liu, W. Zhao, H. Cui, Y. Xie, Y. Wang, T. Xu, F. Huang, Organic–inorganic halide perovskite based solar cells – revolutionary progress in photovoltaics, Inorg. Chem. Front. 2 (2015) 315–335.

[16] T. Zhang, H. Li, H. Ban, Q. Sun, Y. Shen, M. Wang, Efficient CsSnI3-based inorganic perovskite solar cells based on a mesoscopic metal oxide framework via incorporating a donor element, J. Mater. Chem. 8 (2020) 4118–4124.

[17] G. Murtaza, T. Alshahrani, R.M.A. Khalil, Q. Mahmood, T.H. Flemban, H. Althib, A. Laref, Lead Free Double Perovsites Halides X2AgTlCl6 (X = Rb, Cs) for solar cells and renewable energy applications, J. Solid State Chem. 297 (2021), 121988.

[18] T. Ghrib, A. Rached, E. Algrafy, I.A. Al-nauim, H. Albalawi, M.G.B. Ashiq, B. Ul Haq, Q. Mahmood, A new lead free double perovskites K2Ti(Cl/Br)6; a promising materials for optoelectronic and transport properties; probed by DFT, Mater. Chem. Phys. 264 (2021), 124435.

[19] Q. Mahmood, T.I. Al-Muhimeed, A.A. Al Obaid, B. Ul Haq, G. Murtaza, T.H. Flemban, H. Althib, Study of optical and thermoelectric properties of ZYbI3 (Z = Rb, Cs) for solar cells and renewable energy; Modelling by density functional theory, J. Phys. Chem. Solid. 155 (2021), 110117.

[20] Q. Mahmood, M.H. Alhossainy, M.S. Rashid, T.H. Flemban, H. Althib, T. Alshahrani, M. Rashid, A. Laref, First-principles study of lead-free double perovskites Rb2TeX6 (X = Cl, Br, and I) for solar cells and renewable energy, Mater. Sci. Eng., B 266 (2021), 115064.

[21] A. Purkayasth, A.T. Mallajosyula, Optical modelling of tandem solar cells using hybrid organic-inorganic tin perovskite bottom sub-cell, Sol. Energy 218 (2021) 251–261.

[22] D.A. Chalkias, A. Karavioti, A.N. Kalarakis, E. Stathatosa, Unveiling the importance of dripping temperature control of hybrid organic-inorganic perovskite precursor solution for the fabrication of fully ambient air-processed perovskite solar cells, Sol. Energy 224 (2021) 1017–1027.

[23] U. Khan, Y. Zhinong, A.A. Khan, A. Zulfiqar, Q.U. Khan, Organic–inorganic hybrid perovskites based on methylamine lead halide solar cell, Sol. Energy 189 (2019) 421–425.

[24] L. Huang, X. Cui, C. Liu, W. Yang, W. Shi, J. Lai, L. Wang, Improvement on performance of hybrid $CH_3NH_3PbI_{3-x}Cl_x$ perovskite solar cells induced sequential deposition by low pressure assisted solution processing, Sol. Energy 199 (2020) 826–831.

[25] A. Al-Shami, M. Lakhal, M. Hamedoun, A. El Kenz, A. Benyoussef, M. Loulidi, A. Ennaouic, O. Mounkachi, Tuning the optical and electrical properties of orthorhombic hybrid perovskite CH3NH3PbI3 by first-principles simulations: strain-engineering, Solar Energy Mater, Sol. Cell. 180 (2018) 266–270.

[26] G. Volonakis, M.R. Filip, A.A. Haghighirad, N. Sakai, B. Wenger, H.J. Snaith, F. Giustino, Lead-free halide double perovskites via heterovalent substitution of noble metals, J. Phys. Chem. Lett. 7 (7) (2016) 1254–1259.

[27] G. Volonakis, A.A. Haghighirad, R.L. Milot, W.H. Sio, M.R. Filip, B. Wenger, M.B. Johnston, L.M. Herz, H.J. Snaith, F. Giustino, Cs2InAgCl6: a new lead-free halide double perovskite with direct band gap, J. Phys. Chem. Lett. 8 (2017) 772–778.

[28] T.T. Tran, J.R. Panella, J.R. Chamorro, J.R. Morey, T.M. McQueen, Designing indirect–direct bandgap transitions in double perovskites, Mater. Horiz. 4 (4) (2017) 688–693.

[29] E. Haque, M.A. Hossain, Electronic, phonon transport and thermoelectric properties of Cs2InAgCl6 from first-principles study, Comput. Condensed Matter 19 (2019), 00374.

[30] M. Tariq, M.A. Ali, A. Laref, G. Murtaza, Anion replacement effect on the physical properties of metal halide double perovskites Cs2AgInX6 (X = F, Cl, Br, I), Solid State Commun. 314 (2020), 113929.

[31] M. Aslam Khan, H.A. Alburaih, N.A. Noor, A. Dahshan, Comprehensive investigation of Opto-electronic and transport properties of Cs2ScAgX6 (X = Cl, Br, I) for solar cells and thermoelectric applications, Sol. Energy 225 (2021) 122–128.

[32] P.A. Nawaz, G.M. Mustafa, S.S. Iqbal, N.A. Noor, T.S. Ahmad, A. Mahmood, R. Neffati, Theoretical investigations of optoelectronic and transport properties of Rb2YInX6 (X = Cl, Br, I) double perovskite materials for solar cell applications, Sol. Energy 231 (2022) 586–592.

[33] S. Nazir, N.A. Noor, M. Manzoor, A. Dahshan, Ab-initio simulations of Li-based Double Perovksites A2LiInBr6 (A = Rb, Cs) for solar cell applications, Chem. Phys. Lett. 798 (2022), 139612.

[34] R. Anbarasan, M. Srinivasan, R. Suriakarthick, H. Albalawi, J.K. Sundar, P. Ramasamy, Q. Mahmood, Exploring the structural, mechanical, electronic, and optical properties of double perovskites of Cs2AgInX6 (X = Cl, Br, I) by first-principles calculations, J. Solid State Chem. 310 (2022), 123025.

[35] M.W. Mukhtar, M. Ramzan, M. Rashid, G. Naz, M. Imran, F. Fahim, A.A. Al-Obaid, T.I. Al-Muhimeed, Q. Mahmood, New lead-free double perovskites A2NaInI6 (A = Cs, Rb) for solar cells and renewable energy; first principles analysis, Mater. Sci. Eng., B 273 (2021), 115420.

[36] N.A. Noor, M.W. Iqbal, T. Zelai, A. Mahmood, H.M. Shaikh, S.M. Ramay, W. Al-Masry, Analysis of direct band gap A2ScInI6 (A = Rb, Cs) double perovskite halides using DFT approach for renewable energy devices, JMRT 13 (2021) 2491–2500.

[37] S. Iqbal, G.M. Mustafa, M. Asghar, N.A. Noor, M.W. Iqbal, A. Mahmood, Y.H. Shin, Tuning the optoelectronic and thermoelectric characteristics of narrow bandgap Rb2AlInX6 (X= Cl, Br, I) double perovskites: a DFT study, Mater. Sci. Semicond. Process. 143 (2022), 106551.

[38] P. Blaha, K. Schwarz, G.K.H. Madsen, D. Kvasnicka, J. Luitz, Techn. An Augmented Plane Wave+ Local Orbitals Program for Calculating Crystal Properties, 2001.

[39] K. Schwarz, P. Blaha, G.K.H. Madsen, Electronic structure calculations of solids using the WIEN2k package for material sciences, Comput. Phys. Commun. 147 (2002) 71.

[40] M. Petersen, F. Wagner, L. Hufnagel, M. Scheffler, P. Blaha, K. Schwarz, Improving the efficiency of FP-LAPW calculations, Comput. Phys. Commun. 126 (2000) 294–309.

[41] J.P. Perdew, A. Ruzsinszky, G.I. Csonka, O.A. Vydrov, G.E. Scuseria, L.A. Constantin, X. Zhou, K. Burke, Restoring the density-gradient expansion for exchange in solids and surfaces, Phys. Rev. Lett. 100 (2008), 136406.

[42] J.P. Perdew, K. Burke, M. Ernzerhof, Generalized gradient approximation made simple, Phys. Rev. Lett. 77 (1996) 3865.

[43] F. Tran, P. Blaha, Accurate band gaps of semiconductors and insulators with a semi-local exchange-correlation potential, Phys. Rev. Lett. 102 (2009), 226401.

[44] G.K. Madsen, D.J. Singh, BoltzTraP. A code for calculating band-structure dependent quantities, Comput. Phys. Commun. 175 (2006) 67.

[45] M.A. Amin, G. Nazir, Q. Mahmood, J. Alzahrani, N.A. Kattan, A. Mera, H. Mirza, A.M. Moamen, S.R. Adil, A. Gobouria, T. Altalhi, Study of double perovskites X2InSbO6 (X = Sr, Ba) for renewable energy; alternative of organic-inorganic perovskites, JMRT 18 (2022) 4403–4412.

[46] G. Nazir, A. Rehman, S. Hussain, E. Algrafy, Q. Mahmood, A. Mera, H.H. Hegazy, S. Alharthi, M.A. Amin, Study of narrow band gap double perovskites (Sr/Ba) 2BB'O6 (B = In, Tl, B' = Sb, Bi) for optical, thermoelectric, and mechanical properties, J. Mater.Today Commun. 31 (2022), 103547.

[47] A.E. Fedorovskiy, N.A. Drigo, M.K. Naseeruddin, The role of goldschmidt's tolerance factor in the formation of A_2BX_6 double halide perovskites and its optimal range, Small Methods 4 (5) (2019), 1900426.

[48] Q. Mahmood, G. Nazir, S. Bouzgarrou, A.I. Aljameel, A. Rehman, H. Albalawi, B.U. Haq, T. Ghrib, A. Mera, Study of new lead-free double perovskites halides Tl_2TiX_6 (X = Cl, Br, I) for solar cells and renewable energy devices, J. Solid State Chem. 308 (2022), 122887.

[49] T. Zelai, S.A. Rouf, Q. Mahmood, S. Bouzgarrou, M.A. Amin, A.I. Aljameel, T. Ghrib, H.H. Hegazy, A. Mera, First-principles study of lead-free double perovskites Ga_2PdX_6 (X = Cl, Br, and I) for solar cells and renewable energy, JMRT 16 (2022) 631–639.

[50] N. Alaal, I.S. Roqan, Tuning the electronic properties of hexagonal two-dimensional GaN monolayers via doping for enhanced optoelectronic applications, ACS Appl. Nano Mater. 2 (1) (2018) 202–213.

[51] D.R. Penn, Wave-number-dependent dielectric function of semiconductors, Phys. Rev. 128 (1962) 2093.

[52] M. Hassan, I. Arshad, Q. Mahmood, Computational study of electronic, optical, and thermoelectric properties of X_3PbO (X = Ca, Sr, Ba) anti-perovskites, Semicond. Sci. Technol. 32 (2017), 115002.

[53] V.B. Bobrov, S.A. Trigger, G.J.F. van Heijst, P.P.J.M. Schram, Kramers-Kronig relations for the dielectric function and the static conductivity of Coulomb systems, EPL 90 (2010), 10003.

[54] H.C. Wang, P. Pistor, M.A.L. Marques, S. Botti, Double perovskites as p-type conducting transparent semiconductors: a high-throughput search, J. Mater. Chem. 7 (2019), 14705.

[55] Q. Mahmood, T. Zelai, T. Usman, S. Al-Qaisi, M. Morsi, H. Albalawi, A.I. Aljameel, O.A. Alamri, G. Murtaza, First-principles study of lead-free double perovskites $K_2Pt(Cl/Br)_6$ for optoelectronic and renewable energy applications, J. Solid State Chem. 301 (2021), 122294.

[56] T.H. Flemban, V. Singaravelu, A.A.S. Devi, I.S. Roqan, Homogeneous vertical ZnO nanorod arrays with high conductivity on an in situ Gd nanolayer, RSC Adv. 5 (115) (2015) 94670–94678.

[57] Q. Mahmood, M.H. Alhossainy, M.S. Rashid, T.H. Flemban, H. Althib, T. Alshahrani, M. Rashid, A. Laref, First-principles study of lead-free double perovskites Rb2TeX6 (X =Cl, Br, and I) for solar cells and renewable energy, Mater. Sci. Eng., B 266 (2021), 115064.

[58] M. Sajjad, N. Singh, S. Sattar, S. De Wolf, U. Schwingenschlogl, Ultralow lattice thermal conductivity and thermoelectric properties of monolayer Tl2O, ACS Appl. Energy Mater. 2 (2019) 3004–3008.

[59] M. Sajjad, Q. Mahmood, N. Singh, J. Andreas Larsson, Ultralow lattice thermal conductivity in double perovskite Cs_2PtI_6: a promising thermoelectric material, ACS Appl. Energy Mater. 3 (11) (2020) 11293–11299.

[60] G. Zhou, D. Wang, Few-quintuple Bi_2Te_3 nanofilms as potential thermoelectric materials, Sci. Rep. 5 (1) (2015) 8099.

[61] D. Campi, L. Paulatto, G. Fugallo, F. Mauri, M. Bernasconi, First-Principles calculation of lattice thermal conductivity in crystalline phase change materials: GeTe, Sb_2Te_3, and $Ge_2Sb_2Te_5$, Phys. Rev. B 95 (2) (2017), 024311.